Biological Trace Element Research (2020) 196:662–678
https://doi.org/10.1007/s12011-019-01958-2

# Biogenic synthesis of silver nanoparticles using *Gliocladium deliquescens* and their application as household sponge disinfectant

Rasha Mohammad Fathy[1] · Marwa Salah El-deen Salem[2] · Amira Yahia Mahfouz[2]

Received: 5 July 2019 / Accepted: 25 October 2019 / Published online: 6 December 2019


## Abstract

The topic of this investigation was to evaluate the microbial contamination of household sponges, biosynthesize of silver nanoparticles (Ag NPs) by *Gliocladium deliquescens* cell-free supernatant, and estimate the efficiency of Ag NPs as an acceptable disinfectant. The $2^3$ factorial design was applied for the optimization of Ag NPs synthesis. Silver nitrate ($AgNO_3$) concentration was the main positive impact on Ag NP biosynthesis. Various gamma irradiation doses were used in Ag NP production where the highest yield production was at 25.0 kGy. Ag NPs were characterized by UV–Vis. spectroscopy, The Fourier-transform infrared spectroscopy analysis (FTIR), dynamic light scattering (DLS), X-ray diffraction (XRD), and transmission electron microscope (TEM). Ag NPs were monodispersed spherical-shaped with 9.68 nm mean size. Two hundred sponge samples that were collected from different Egyptian household furniture and kitchens were highly contaminated by various contaminants including *Salmonella* spp., *Staphylococcus* spp., coliform bacteria, Gram-negative bacteria, yeasts, and molds. Ag NPs showed functional antimicrobial activity against all the microbial contaminants; *Salmonella* spp. was completely inhibited by Ag NP (50.0 μg/mL) treatment. The Ag NPs have the maximum inhibition zone against *Salmonella* spp. (14 mm) compared with the *Staphylococcus* spp. (12.3 mm). The minimum inhibitory concentration (MIC) of Ag NPs against *Salmonella* spp. and *Staphylococcus* spp. were 6.25 μg/ mL and 12.5 μg/ mL, respectively. The antibiofilm activity of Ag NPs was the highest at the concentration of 50.0 μg/mL recording 63.3 % for *Salmonella* spp. and 54.5 % for *Staphylococcus* spp. Ag NPs may find potent disinfectant applications for household purposes.

**Keywords** Silver nanoparticles · *Gliocladium deliquescens* · Gamma irradiation · Silver antimicrobial activity · *Salmonella* spp. · *Staphylococcus* spp

## Introduction

Nanotechnology is one of the most dynamic subjects of research in recent material sciences; therefore, metal nanoparticles have a great consideration with respect to their physicochemical properties and exclusive optoelectronic with applications in multiple areas such as drug delivery, electronic sensing, and catalysis [1].

Numerous studies have confirmed the efficiency of silver nanoparticles (Ag NPs) as a curative device for covering burns and they were also integrated into clothing for use as an antimicrobial during manufacturing [2]. Ag NPs are the most broadly used nanomaterials in the healthcare field today, with worldwide production annually approximate to be in the area of 500 tons [3].

Ag NP production by means of fungi has various advantages. They include large-scale synthesis of nanoparticles by easy technique, great dispersion of the synthesized nanoparticles, and higher amounts of protein expressions. One of the inherent implementations of silver is its use as a disinfectant of industrial materials. The antimicrobial effect of Ag NPs is attributed to its activity on the mycelia and colonies of the pathogenic organisms [4]. Ag NPs have been used broadly in multiple fields as antibacterial where the antimicrobial effectiveness of Ag NPs was well displayed and several mechanisms for their biocidal effects have been suggested [5].

✉ Rasha Mohammad Fathy
rasha.elhadad@eaea.org.eg; rashafathy82@gmail.com

[1] Drug Radiation Research Department, National Center for Radiation Research and Technology (NCRRT), Atomic Energy Authority, P.O Box 29, Nasr City, Cairo, Egypt

[2] Botany and Microbiology Department, Faculty of Science (Girls), Al-Azhar University, Cairo, Egypt

Ag NPs could act as a leader in the fight toward pathogenic microbes. The high surface area of Ag NPs is accountable for their potent antimicrobial action in contrast to the bulk structure of silver because of the greater contact of nanoparticles with microorganisms. Ag NPs are efficient against a wide spectrum of Gram-positive and Gram-negative bacteria and various antibiotic-resistant strains [6, 7]. Ag NPs attracted the attentions of numerous industrial areas particularly when an antiseptic effect is desirable including food, medicine, textile, pharmacy, cosmetology, construction, and industrial branches [8]. They also utilized in the power industry and in the biomedicine as receptors in the labeling of biological elements [9]. Ag NPs are commonly incorporated into the structure of textile and household materials to minimize or prevent the microbial growth for the production of sterile materials [10]. Ag NPs may be synthesized by gamma irradiation that considered a clean and simple method and provides a potent mean for metal ions reduction [11].

Considering 2015 The World Health Organization estimation, *Salmonella* is one of the main food-borne illness causes resulted in 230,000 deaths cases [12]. Symptoms of *Salmonella* infection that appear normally after 12–72 h of contaminated foods ingestion were recognized as abdominal pains, vomiting, fever, diarrhea, weakness, and appetite loss [13].

The aim of this research was to assess the antimicrobial impact of Ag NPs against various microbial strains isolated from household environments to get better utilization of nanoparticles for specific antimicrobial applications.

## Experimental Methods

All experiments during this study were carried out in the Drug Microbiology laboratory, Drug Research Department, National Centre for Radiation Research and Technology (NCRRT), Atomic Energy Authority and Botany and Microbiology Department, Faculty of Science (Girls), Al-Azhar University, Cairo, Egypt at 2018.

## Chemicals

All chemicals used in the present study were of analytical grade and were manufactured by Sigma-Aldrich at Abou Zer El Ghefari Street, Al Hay El Sabea, Nasr City, Cairo Governorate, Egypt.

## Fungal Strain

The fungal strain, *G. deliquescens*, was provided friendly from the Drug Microbiology laboratory, Drug Research Department, National Centre for Radiation Research and Technology (NCRRT), Atomic Energy Authority. The fungal strain was maintained on a potato dextrose agar medium at 4 °C and subcultured every month.

## Biosynthesis of Ag NPs

The fungal strain, *G. deliquescens*, was utilized for biosynthesizing Ag NPs. Sterile glucose yeast peptone (GYP) medium broth containing (g/L) yeast extract 3, glucose 10, and peptone 5 was inoculated with *G. deliquescens* and incubated aerobically with shaking (180 rpm) at 28 °C. After 72 h incubation period, the culture samples were filtrated with filter paper (Whatman no.1) followed by the centrifugation at 5000 rpm for 10 min, and the resulted supernatants were utilized in the synthesis of Ag NPs. An aqueous solution of 1 mM $AgNO_3$ (5 mL) was blended with 5 mL of fungal supernatant then agitated with darkness at 25 °C for 24 h. The control without $AgNO_3$ was run with the experiment by the same conditions [14].

## Two-Level Factorial Design

The $2^3$ factorial design was applied to examine if the main significant parameters affect Ag NP production. For modeling design and statistical calculations, Version 7.1 of Design-Expert® Software statistical software package from Stat-Ease Inc., Minneapolis, MN, USA, was used. Optimization of Ag NP synthesis using the statistical procedure is a paramount impact demanded to estimate the valid conditions for the high-scale synthesis of Ag NPs.

The factors (independent factors) used through the study that may affect Ag NPs synthesis were, namely, $AgNO_3$ concentration (1 and 2 mM), the ratio of supernatant: $AgNO_3$ (v:v), and the incubation time (h).

In this study, 16 runs were used to evaluate 3 variables where each variable was examined in two levels, low level ($AgNO_3$ concentration at concentration 1 mM, the ratio of filtrate: $AgNO_3$ (1:1) and the incubation time 24 h) and high level ($AgNO_3$ concentration at concentration 2 mM the ratio of filtrate: $AgNO_3$ (1:2) and the incubation time 48 h). The experiments were executed in duplicate and all the flasks were held at 150 rpm in shaking incubator in the dark. Control (has not contained silver ions) was similarly run with the test runs. After conducting experiments, UV absorbance in nanometer (dependent factor) was observed as a response that indicates Ag NP synthesis. From the Pareto chart is a vertical bar graph in which values are plotted in decreasing order of relative frequency and clearly illustrate which variables have the greatest cumulative effect on Ag NPs [15] and normal plot analysis, the parameters which display the highly positive

effect were considered to have a greater influence on Ag NP production. The quality of the obtained model was expressed by the coefficient of determination ($r^2$), the value of adjusted-$r^2$ of the model, standard error of the estimate (SE), and Fisher ratio value ($F$) [16].

## Irradiation Process

The operation of irradiation was performed at the National Centre for Radiation Research and Technology (NCRRT). The facility used was $^{60}$Co-Canadian Gamma Cell Ge220. Irradiation was executed at a dose rate of 1.58 kGy/h by the course of the experiment under ambient conditions. Specimens were irradiated at: 1.0, 5.0, 10.0, 15.0, 20.0, 25.0, and 30.0 kGy [17].

## Characterization of Ag NPs

Characterization of Ag NPs was emphasized by UV–Vis. spectrophotometer (T60 U-UV-Vis-UK). The blank was prepared by using a cell-free supernatant with distilled water instead of $AgNO_3$ solution. Samples were sonicated for 20 min before analysis. The Fourier-transform infrared spectroscopy analysis was performed by FTIR-Vertex 70 spectrometer Bruker-Germany using dehydrated potassium bromide (KBr) pellets that pressed mechanically with dried Ag NPs [18]. The average size of particles and particles distribution were estimated by dynamic light scattering (DLS-PSS-NICOMP 80-ZLS particle sizing system, St. Barbara, CA, USA). The X-ray diffraction pattern was analyzed by the XRD 6000 series, including residual crystallite size/lattice strain and crystal nature by overlaying X-ray diffraction patterns Shimadzu apparatus using Cu-K(α) (copper-potassium (alpha) target of wavelength 1.5418 Å and nickel filter Shimadzu Scientific Instruments (SSI), Tokyo, Japan. Transmission electron microscopy (TEM- JOEL JEM 100 CX-Japan) sample was prepared by dropping the Ag NP colloidal solution on the carbon-coated copper grid then allowing evaporation at room temperature to estimate the morphology and size of the biosynthesized Ag NPs.

## Isolation of Bacteria and Fungi from the Different Collected Sponge Samples

Two hundred furniture and local kitchens sponges samples were collected in clean and sterile plastic bags from four governorates in Egypt; Cairo, Giza, El-Behera, and Al-Qalubya. Isolation was performed according to [19] where 1 g of each sponge sample was weighted and cut into small cubes. The cubes were grounded into a fine powder then blended with 99 mL sterile peptone water medium that contains (g/L) peptone 10.0 and NaCl 5.0; then, it was stirred on a shaker for 1 h to be homogenized. From $10^{-1}$ to $10^{-5}$ serial dilutions of every sponge samples; 100 μL was inoculated into sterile Petri dishes contains 15 mL of nutrient agar medium for bacteria and potato dextrose agar for fungi. The media then were mixed well with the added sponge sample inoculums and let to solidify. The bacterial isolation plates were incubated at 37 °C for 24 hours while the fungal isolation plates were at 28 °C for 5–7 days. The total counts for both bacteria and fungi were registered at the termination of the incubation time. The selective media used in the enumeration of different microbial contaminants of sponge samples were as follows: Violet Red Agar medium was used for Coliform bacteria [20] and Colbeck Egg-Yolk agar medium was used for *Staphylococcus* spp. [21], While MacConkey agar was used for *Salmonella* spp. [22] and finally, Eosin Methylene Blue agar for Gram-negative bacteria [23].

## Ag NP Treatment of the Contaminated Sponge Samples

Heavily contaminated sponge samples were prepared as the previous method as they were weighted, cut with a clean sharp scissors in small cubes and then the cubes were grounded into a fine powder and finally added to the Ag NP (50 μg/mL) colloidal solution. The total microbial counts of treated sponge specimens were calculated to define the antimicrobial performance of Ag NPs. Regarding the morphological and physiological features as Gram-reaction, motility, spore stain, and pigment production, the bacterial isolates were identified to different species. The reduction rate (%) of the samples was estimated according to Eq. 1 in [24]:

$$\text{Reduction}\% = \frac{\text{Total count}\left(\frac{\text{CFU}}{\text{mL}}\right)\text{of control} - \text{Total count}\left(\frac{\text{CFU}}{\text{mL}}\right)\text{of treated Ag NPs}}{\text{Total count}\left(\frac{\text{CFU}}{\text{mL}}\right)\text{of control}} \times 100 \quad (1)$$

CFU/mL (colony-forming unit/mL) is a unit used to estimate the number of viable bacteria or fungal colonies in milliliter of the sample.

## The Antibacterial Potency of Ag NPs on *Salmonella* spp. and *Staphylococcus* spp.

### Disk Diffusion Test

Disk diffusion technique was employed to evaluate the effects of Ag NPs on *Salmonella* spp. and *Staphylococcus* spp. in accordance with [25]. To study the antibacterial influence of

Ag NPs by a disk diffusion method, bacterial suspension was prepared and adjusted to standard 0.5 McFarland's concentration. Bacteria were inoculated on a nutrient agar medium. On every nutrient agar plate surface, three sterilized filter paper disks that dippedin 10 μL of, Ag NPs (50 μg/mL), fungal cell-free supernatant (negative controls), and amoxicillin/clavulanate 20/10 μg/mL (positive controls) were used. The plates were incubated at 37 °C. The microbial cloud lack of growth was observed after 24 h and represented as a zone of inhibition in millimeter.

### Analysis of Minimum Inhibitory and Bactericidal Concentrations (MIC, MBC) of Ag NPs

The MIC and MBC of Ag NPs against *Salmonella* spp. and *Staphylococcus* spp. were estimated using the well diffusion method. Overnight, *Salmonella* and *Staphylococcus* cultures were incubated for 2 h at 37°C. After that, the inoculum of the tested bacteria was adjusted at 0.5 McFarland (1–2) × $10^8$ CFU/mL, using UV–Vis. spectrophotometer at 600 nm. An amount of 100 μL McFarland's bacterial suspension was inoculated into Petri dish plates containing plate count agar medium. Ag NPs were serially diluted two-fold with sterile distilled water to concentrations of 50.0, 25.0, 12.5, 6.25, and 3.12 μg/mL and applied upon *Salmonella* spp. and *Staphylococcus* spp. The plates were incubated at 37 ° C for 24 h and the zone of inhibition was determined in millimeter [26]. MIC was defined as the minimum concentration of Ag NPs that will inhibit the obvious growth of bacteria after overnight incubation while MBC is the minimum concentration that exhibits a predetermined reduction (99.9%) when related to the MIC dilution.

### The Antibiofilm Activity of the Biosynthesized Ag NPs

Ag NPs (50.0 μg/mL) synthesized through *G. deliquescens* cell-free supernatant with the assistance of 25.0 kGy gamma irradiation was tested for their antibiofilm capacity against *Salmonella* spp. and *Staphylococcus* spp. by tubes method as described by [27]. Five milliliters of the nutrient broth were added in test tubes, and inoculated with 10 μL of 0.5 McFarland (1 × $10^8$ CFU/mL) examined bacteria. 0.5 mL of Ag NPs (50.0 μg/mL) was included in the test tubes while the same amount of water was included in the control tubes. The tubes were incubated at 37 °C for 24 h. After incubation period, the contents of the media in both the Ag NPs-treated and the control tubes were eliminated. The tubes were treated with phosphate buffer saline (PBS), pH 7 and lastly dehydrated. An amount of 5.0 mL sodium acetate (3.0 %) was utilized to stabilize the adherent bacterial layers for 10 min then washed with deionized water. The biofilms of the examined bacteria were stained with crystal violet (0.1%) for 15 min and then rinsed with de-ionized water to excrete the residue of the dye. For dissolving the crystal violet stain, 2.0 mL of ethanol was added to each tube. The provided biofilm was convinced if a notable stained layer was identified on the tube (surface and the bottom). The biofilms of bacteria were quantitatively evaluated by UV–Vis. spectrophotometer at 570 nm. The percentage of inhibition was assessed using Eq. 2 according to [28].

$$\text{Inhibition}\,\% = \frac{\text{ODc} - \text{ODt}}{\text{ODc}} \times 100 \quad (2)$$

where; ODc is the absorbance of the control sample (without Ag NPs) and ODt is the absorbance of the Ag NP-treated samples.

### Comparison of the Fourier-Transform Infrared Spectra

FTIR measurements were performed to untreated and Ag NPs *Salmonella* spp. and *Staphylococcus* spp. dried cells to detect the changes in the wave number and transmittance % occurred due to Ag NPs binding to the bacterial cells. Before analyzing, a few milligrams of each bacterial pellets were grounded and mixed well with KBr provided the concentration of 2%. Prprocessing has occurred at total spectral region of (400 to 4000 $cm^{-1}$). The background was obtained, corresponding to pure KBr, was subtracted from each sample spectrum [29].

### Interpretation of the Action of Ag NPs on the Bacteria by the Scanning Electron Microscope

Visualization of *Salmonella* spp. and *Staphylococcus* spp. after contact with Ag NPs was also developed using scanning electron microscope (SEM-JEOL-JSM2500-Japan) by the following procedure according to [30]. *Salmonella* spp. and *Staphylococcus* spp. cultures were incubated with Ag NPs (50.0 μg/mL) at 37 ± 1 °C in an incubating shaker at 150 rpm for 24 h. Next, bacteria were rinsed three times with phosphate-buffered saline (PBS) and then dehydrated in ethanol solutions for 15 min. Consequently, dried bacterial cells were coated with carbon and imagined in SEM.

## Statistical Analysis

All results were analyzed by one-way ANOVA at $p < 0.05$ and designated as mean ± SD. Least significant difference (LSD) values of the results were reported. Duncan's test was used to compare between treatment groups where means bearing different superscripts differ significantly ($p < 0.05$) by Duncan's multiple range test [31]. The data were analyzed by IBM Corp (Released 2016. IBM SPSS Statistics for Windows, Version 24.0. Armonk, NY: IBM Corp).

## Results and Discussion

### Synthesis and Characterization of Ag Nanoparticles

#### Biosynthesis of Ag NPs

This investigation discussed a method to produce Ag NPs utilizing *G. deliquesecens* cell-free supernatant. The capacity of fungi to uptake, collect, and reduce heavy metals may offer technologies based on microbes for metal replacement or friendly environmental synthesizing of metal nanoparticles that are considered an economic strategy and protection of the environment [32]. This fungal-mediated green synthesis of Ag NPs could be scaled up and adopted for health care and sterilization purposes such as detection and treatments of cancer [33]. The absorbance peak of Ag NPs reveals their characteristic features as the shape and size [34].

The fungal cell-free supernatant of *G. deliquesecns* was mixed to $AgNO_3$ solution and after 24 h the color was changed from yellow to reddish-brown indicating the production development of Ag NPs at room temperature as explained in Fig. 1. The changing of color means that the aqueous $Ag^+$ was reduced to $Ag^0$. The absorption spectrum of the mixture was scanned in the range of 200–800 nm. The UV–Vis. spectra attested the maximum absorbance 0.459 at 435 nm which is a specific characteristic peak of Ag NPs. The amino acids play an essential role in the stabilization of the nanoparticles where they form a capping layer around nanoparticles preventing their aggregation.

The excitation of light on the metal surface is a specific characteristic for each metal that is called surface plasmon resonance (PSR) and resulting from a monochromatic light source brightens onto the nanoparticles causing conduction electrons oscillation toward the preparation of anionic metal core [17]. The area of the peak absorption could be correlated with the shape and particle size [35].

The nanoparticle synthesis with fungi has multiple benefits, e.g., the fungi could be cultured and grown in an easy way and they are safe to handle, also fungi have metabolites that might help in a reduction of metals to form nanoparticles. Moreover, they have innumerable applications [36, 37]. Ag NPs may be commonly introduced into various consumer products as disinfectants particularly when the expansion of nanotechnology is in progress [38].

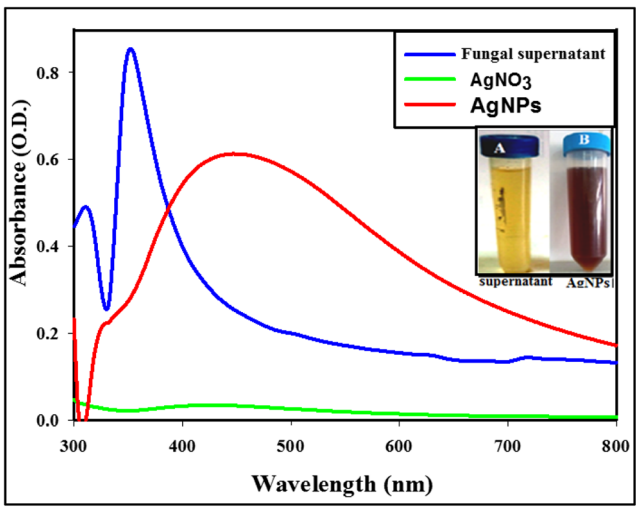


**Fig. 1** UV-Vis. spectrum of *G. deliquescens* supernatant, $AgNO_3$, and Ag NPs synthesized using cell-free supernatant of *G. deliquescens*

#### Two-level factorial design

Various experimental conditions have been studied to recognize their effect on the bioreduction of silver ions into Ag NPs colloidal solutions.

The regular optimization has been performed by observing the effect of one parameter factor at the point on the tested response where one parameter factor is changed; the other factors are stable at a constant level. This routine does not distinguish the access conclusions involved among the examined factors and the total force of the parameter factors on the test response. So, the mentioned Ag NP biosynthesis factors that may affect the production rate were examined according to a 2-level design (Table 1).The $2^3$ factorial design has been practiced to appraise the notable effect of $AgNO_3$ concentration (mM), the ratio of fungal cell-free supernatant to $AgNO_3$ solution (v:v), and the incubation times of the mixture on the production of Ag NPs by *G. deliquescens*. Besides, in this procedure when the number of trials required for ensuring the results increases this may improve the expenses and time [39].

All experimental trials were assayed at 435 nm according to the previous test. The response of the analysis was defined as the absorbance (nm) that reflects Ag NP production. The high absorbance means high Ag NP production. In general, all the experiments were accomplished in triplicate and the absorbance average was considered. The response of Ag NP synthesis at 16 runs experimental set-up was shown in Table 1.

The results of 16 runs of the three tested variables confirmed that Ag NP formation was markedly increased at trial 15 where the maximum bioreduction rate of Ag NPs with the condition of $AgNO_3$ concentration (1 mM), 1:1 (v:v) ratio of fungal cell -free supernatant to $AgNO_3$ and 48 h incubation time. The recorded absorbance was 1.037 nm. While the least absorbance value was 0.165 nm at trial 3 with the condition of $AgNO_3$ concentration (2 mM), 1: 1 (v:v) ratio of fungal cell-free supernatant to $AgNO_3$ and 48 h incubation time. The $r^2$ value contributed a standard of whence considerable variability in the detected response values could be demonstrated by the test factors. The $r^2$ value is constantly within 0 and 1. The

**Table 1** The experimental conditions for $2^3$ factorial design and the absorbance for Ag NP biosynthesis

| Run no. | $AgNO_3$ conc. (mM) | Rati (fungal supernatant: $AgNO_3$) | Incubation time (h) | Absorbance at 435 nm |
|---|---|---|---|---|
| 1 | 1 | 1:2 | 24 | $0.580^{f} \pm 0.001$ |
| 2 | 1 | 1:2 | 48 | $0.386^{c} \pm 0.022$ |
| 3 | 2 | 1:1 | 48 | $0.165^{a} \pm 0.015$ |
| 4 | 2 | 1:2 | 48 | $0.359^{c} \pm 0.017$ |
| 5 | 2 | 1:2 | 24 | $0.525^{b} \pm 0.015$ |
| 6 | 1 | 1:2 | 24 | $0.948^{i} \pm 0.001$ |
| 7 | 1 | 1:1 | 48 | $0.732^{h} \pm 0.016$ |
| 8 | 2 | 1:2 | 24 | $0.483^{e} \pm 0.012$ |
| 9 | 1 | 1:1 | 24 | $1.007^{j} \pm 0.012$ |
| 10 | 2 | 1:2 | 48 | $0.658^{g} \pm 0.016$ |
| 11 | 1 | 1:1 | 24 | $0.749^{g} \pm 0.011$ |
| 12 | 2 | 1:1 | 24 | $0.409^{d} \pm 0.030$ |
| 13 | 2 | 1:1 | 24 | $0.567^{f} \pm 0.020$ |
| 14 | 2 | 1:1 | 48 | $0.485^{e} \pm 0.021$ |
| 15 | 1 | 1:1 | 48 | $1.037^{k} \pm 0.029$ |
| 16 | 1 | 1:2 | 48 | $0.194^{a} \pm 0.022$ |
| LSD | — | — | — | 0.040 |

The results are described as mean ± SD. LSD: least significant difference. Means bearing different superscripts differ significantly ($p < 0.05$) by Duncan's multiple range test

closer $r^2$ to 1, the more effective the model and is the choice to foretell the response [40].

Statistical analysis of this design (Table 2) and normal plot (Fig 2a) illustrated that the most positive impact on optimization conditions of Ag NP production was $AgNO_3$ concentration. $AgNO_3$ at 1 mM concentration was more effective recording the highest absorbance value that showed the highest yield production of Ag NPs.

Moreover, the other two parameters; ratio of the fungal supernatant to $AgNO_3$ solution and incubation time has no great effect on Ag NP production. The regression analyses practiced on the tested data, the variables of the test, and the variable response were associated with the later model (Eq. 3) terms of coded factors:

$$\begin{aligned}\text{Ag NP production} = {} & +0.58 + 0.12\text{A} - 0.067\text{B} - \\ & 0.078\text{C} - 0.11\text{AB} - 0.042\text{AC} - \\ & 0.043\text{BC} - 0.081\text{ABC}\end{aligned} \tag{3}$$

The quadratic equation model was verified, by the Design-Expert 7.0, trial version for ANOVA and the results were presented in Table 2.

The influence of the individual parameters analyzed in Plackett–Burman Design is assembled as a Pareto chart that described the degree of the variables significance that may be required in Ag NP production (Fig 2b). The effective factor of the experimental design was $AgNO_3$ concentration.

From 16 trials, trial no 15 reported the highest Ag NP production. So, we tested the impact of gamma irradiation on Ag NPs production by the same synthesis conditions of trial 15.

### Synthesis of Ag NPs by gamma irradiation

*G. deliquescens* cell-free supernatant and $AgNO_3$ mixture were subjected to different gamma irradiation doses: 1.0, 5.0, 10.0, 15.0, 20.0, 25.0, and 30.0 kGy to define the competence of gamma irradiation in Ag NP synthesizing. Ag NPs were characterized by UV–Vis. spectrophotometer in the range of 260–800 nm. It was observed that as the gamma irradiation dose was increased, Ag NP concentration was also enhanced. Gamma irradiation was deeply effective in stimulation of Ag NP production. After irradiation, the density of the yellowish-brown color of solution that initially indicated Ag NP formation was highly intense so that samples were diluted with deionized water in the proportion of 1:3 (v:v). Ag NPs were extremely stable. The specific plasmon resonance absorption bands of Ag NPs were detected at between 405 and 415 nm according to the irradiation dose. The irradiation approach provides numerous advantages; a clean and more convenient method for metal nanoparticles preparation.

The specific surface plasmon resonance (SPR) is a phenomenon that occur at the metal surfaces when an incident light beams tricks the surface at a specific angle resulting in a graded reduction in the reflected light intensity. SPR for the greatest Ag NP yield production was detected using 25.0 kGy

**Table 2** Analysis of variance (ANOVA) for Ag NP production

| Source | Sum of squares | DF | Mean square | *F* value | $r^2$ | SD |
|---|---|---|---|---|---|---|
| Model | 0.77 | 7 | 0.11 | 2.23 | 0.7389 | 0.18 |
| A-$AgNO_3$ conc. | 0.23 | 1 | 0.23 | 6.80 | | |
| B-ratio | 0.072 | 1 | 0.072 | 2.13 | | |
| C-time | 0.098 | 1 | 0.098 | 2.88 | | |
| AB | 0.21 | 1 | 0.21 | 6.05 | | |
| AC | 0.029 | 1 | 0.029 | 0.84 | | |
| BC | 0.029 | 1 | 0.029 | 0.86 | | |
| ABC | 0.10 | 1 | 0.10 | 3.08 | | |
| Pure error | 0.27 | 8 | 0.034 | | | |
| Cor total | 1.04 | 15 | | | | |

to be 4.356 nm at 405 nm. On the other hand, the irradiation over than 25.0 kGy caused a reduction in Ag NP production as presented in Table 3.

In the aquatic solution, $AgNO_3$ was separated into $Ag^+$ and $NO^{-3}$ ions. The radiolytic process of water due to ionizing radiation explained by [41] occurs in three principal steps happen on regular time scales: (1) The *physical stage*, which is performed after the initial matter-ionizing radiation interaction about 1 femto second, leading to the formation of ionized water molecules ($H_2O^+$), excited water molecules ($H_2O^*$), and subexcitation electrons ($e^-$). (2) The *physico-chemical stage at* $10^{-0p}$–$10^{-10}$ s where numorous processes occur, including ion-molecule reaction, dissociative relaxation, autoionization of excited states, and thermalization of subexcitation electrons (solvation of electrons). (3) During the *chemical stage at* $10^{-0e}$–$10^{-1}$ s, the species react in the paths and diffuse in solution. Then they react with each other and further with surrounding molecules (in the solution). The path of the particles grows on account of the diffusion of radicals and their consequent chemical reactions. These species could have a powerful reduction of $Ag^+$ into $Ag^0$ to avoid using of additional reducing factors as attested in Eq. 4. Furthermore, $Ag^0$ nuclei amount can be dominated by varying the gamma irradiation dose (Eq. 5) [42].

$$H_2O \rightarrow^{\gamma-\text{irradiation}} e^-_{aq}, H_3O^+, H^\bullet, OH^\bullet \quad (4)$$

$$Ag^+ + e^-_{aq} + H^\bullet \rightarrow^{\text{reduction}} Ag^0 + H^+ \quad (5)$$

The germination of Ag NPs by reduction of $Ag^+$ to $Ag^0$ has occurred in ordered stepwise manner. Silver atoms created by the irradiation combined into oligomers. The aqueous hydrated electrons rapidly merged to silver ions to form a dimer, trimer, tetramer. and an elevated array of silver ion bunches ($Ag^{+n+1}$). After that, the clusters aggregated into larger metallic bunches and nanoparticles. The hydrated electrons reacted with an excess of $Ag^+$ clusters to produce the approximately stabilized $Ag^0$ clusters as evidenced in (Eq. 6 and 7) [43].

$$Ag^+ Ag^0 + nAg^+ \rightarrow 2\,(Ag^+)_n \quad (6)$$

$$(Ag^+)_n + n\,e^-_{aq} \rightarrow (Ag^0)_n \quad (7)$$

In our study, Ag NPs and the metallic clusters grew by gamma irradiation are capped and protected by the

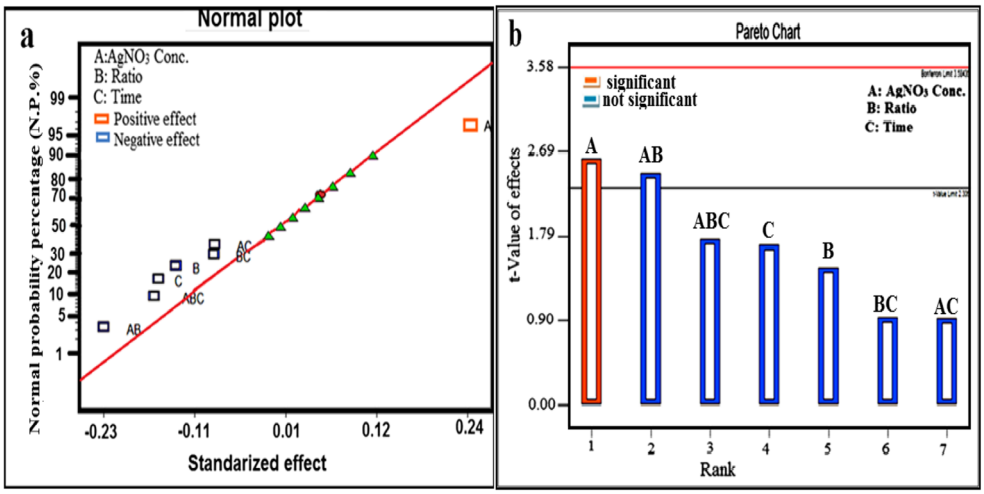


**Fig. 2** The effect of individual parameters on Ag NP production. **a** Normal plot and **b** Pareto chart (The letters that represented the tested variables where A: $AgNO_3$ concentration, B: the ratio of supernatant: $AgNO_3$ (v:v), and C: incubation time. The orange columns represented the positive effect while the blue columns represented the negative effect. The most effective parameter is $AgNO_3$ concentration).

**Table 3** Effect of different gamma irradiation doses on Ag NPs synthesis by *G. deliquescens* cell free-supernatant

| Gamma irradiation doses (kGy) | Wavelength (nm) | Absorbance (optical density) |
|---|---|---|
| 1.0 | 405 | $1.092^{a} \pm 0.044$ |
| 5.0 | 410 | $1.473^{b} \pm 0.018$ |
| 10.0 | 410 | $2.256^{c} \pm 0.023$ |
| 15.0 | 415 | $3.675^{d} \pm 0.013$ |
| 20.0 | 405 | $4.299^{f} \pm 0.060$ |
| 25.0 | 405 | $4.356^{g} \pm 0.063$ |
| 30.0 | 405 | $3.849^{e} \pm 0.029$ |
| LSD | — | 0.427 |

The results are described as mean ± SD. LSD: least significant difference. Means bearing different superscripts differ significantly ($p < 0.05$) by Duncan's multiple range test

protein of the fungal cell-free supernatant. The binding of Ag NPs to the protein is likely achieved through Ag–O bonding[14].

## Characterization of the Synthesized Ag NPs

FTIR spectrum shown in Fig. 3a was performed to differentiate the functional groups qualified for synthesis and stabilization of Ag NPs. The spectra were accomplished by forming a KBr disk with Ag NPs produced using *G. deliquscens* cell-free supernatant that irradiated at 25.0 kGy. Also, FTIR analysis was carried out to identify the reasonable interactions between Ag NPs and bioactive particles, which might be accountable for the formulation and stabilization (capping agent) of Ag NPs [44]. Nanoparticles could attach to proteins through cysteine residues or free amine groups; therefore, the proteins in the cell-free supernatant may cause stabilization of the Ag NPs [34, 45] (Fig. 3a).

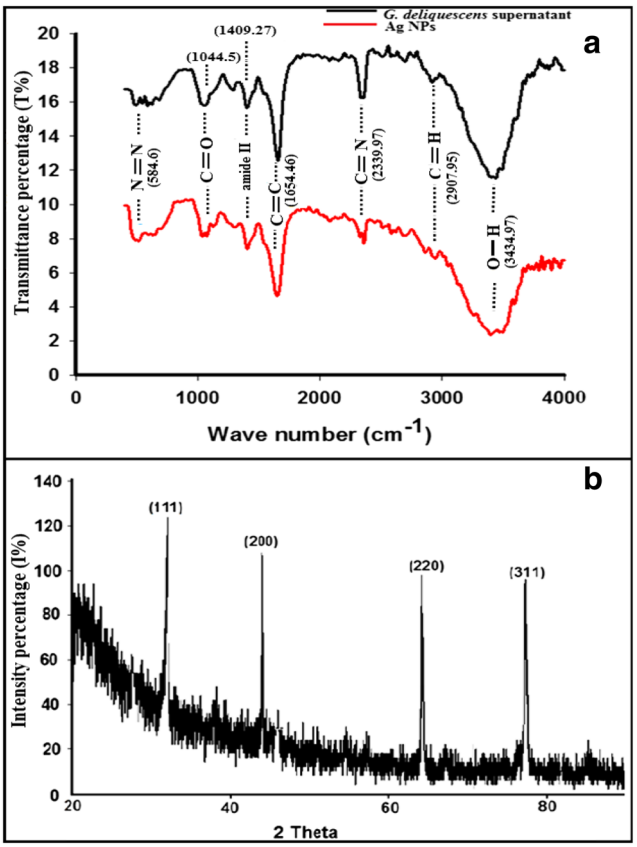


**Fig. 3** Characterization of Ag NPs synthesized using cell-free supernatant of *G. deliquescens* and 25.0 kGy gamma irradiation dose. **a** FTIR spectra. **b** XRD pattern

By comparing FTIR spectrums of both *G. deliquescens* cell-free supernatant and Ag NPs synthesized by *G. deliquescens* cell-free supernatant at 25.0 kGy, there were no changes in all peaks position, but little changes in transmittance % had been noted. These changes in transmittance % may be attributed to Ag-O negatively charged hydroxyl groups conjugated with Ag NPs with–OH groups including in reduction process [32].

The peak appeared at 3434.97 $cm^{-1}$could be assigned to a strong stretching vibration of the hydroxyl functional group according to [46]. The other peaks at 2907.95 and 2339.97 $cm^{-1}$ are assigned to C-H or C=N double bond, respectively, while, the peak at 1654.46 $cm^{-1}$ may be regarded to C=C stretch [47]. The peaks of absorbance at 1409.27 $cm^{-1}$ resembled the amide II group; however, the peak at 1044.5 $cm^{-1}$could be agreed with carbonyl (C–O–) stretching vibrations in the protein amide linkages [48]. The peaks noticed at 552.2, 548.6, and 470.8 $cm^{-1}$ showed agreement with N=N vibration [49].

Fig.3b presented the XRD pattern of Ag NPs synthesized using 25.0 kGy gamma-irradiated *G. deliquescens* cell-free supernatant. The XRD pattern showed intense peaks of Bragg's reflection range from 20 to 80 of 2θ values corresponding to (111), (200), (220), and (311) set based on the face-centered cubic structure of Ag NPs. The XRD pattern demonstrated the biosynthesized Ag NPs in the form of nanocrystals.

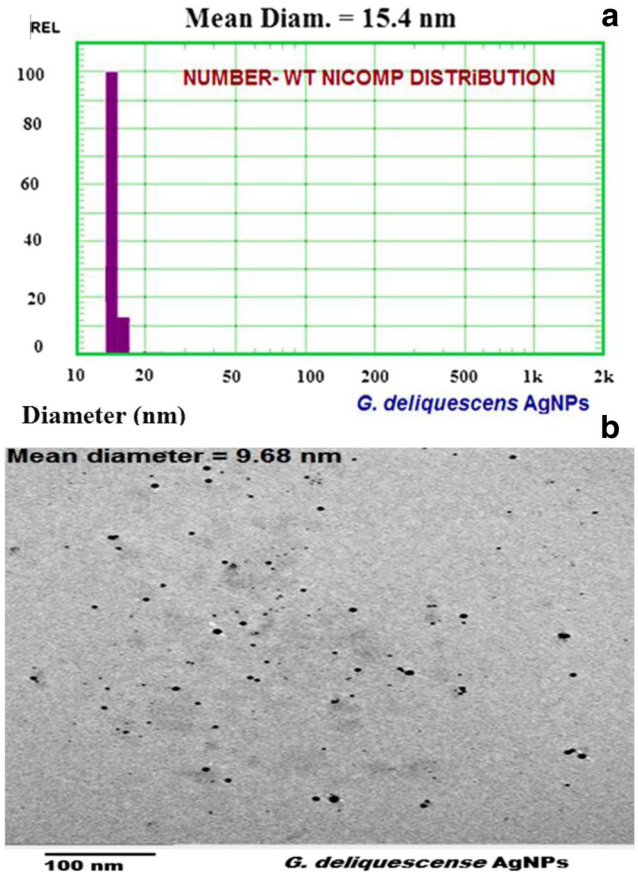


**Fig. 4** Validation of Ag NPs synthesized using cell-free supernatant of *G. deliquescens* and 25.0 kGy gamma irradiation dose. **a** Dynamic light scattering analysis showed that the average particle size distribution of Ag NPs was 15.4 nm. **b** Transmission electron microscope image showed Ag NP mean particles size of 9.68 nm. Number-weighted Nicomp distribution means the relative proportion of number of differently sized particles occupied by differently sized particles; Nicomp is the DLS apparatus model.

The results have been verified with dynamic light scattering examination (DLS) as displayed in Fig 4a where the average of the particle size distribution of Ag NPs was 15.4 nm.

Transmission electron microscope (TEM) analysis demonstrated the mean particle size and size distribution. TEM micrograph showed spherical monodispersed nanoparticles with a mean particles size of 9.68 nm (Fig. 4b).

### The Antimicrobial Action of Ag NPs

The furniture and local kitchens household sponge samples were collected from four governorates in Egypt; Cairo, El-Giza, Al-Qalubya, and, El-Behera. The furniture samples were divided into ten groups while kitchen samples were differentiated into three groups according to diverse source collections. The total counts of bacteria, molds, and yeasts isolated from furniture and local kitchens household sponge samples (untreated and treated with Ag NPs (50.0 μg/mL) were illustrated in (Table 4).

The results showed that the untreated (control) furniture sponges that did not receive any disinfectant treatment were heavily contaminated and the largest bacterial counts were recorded with group 9 and 6 ($67 \times 10^5$ and $55 \times 10^5$ CFU/mL, respectively). Fungal isolates were not identified. Otherwise, kitchen sponges specimens were less contaminated where the elevated bacterial total count was with group 2 ($57 \times 10^5$ CFU/mL). The fungal isolates were recognized from kitchen sponge groups. Group 1 represented the highest molds total count was $3 \times 10^3$ (CFU/mL), in contrast, the highest yeast total count was estimated for group 2 ($4 \times 10^3$ CFU/mL). The specimens treated by Ag NPs (50.0 μg/mL) exhibited an excellent reduction in total counts for bacteria, molds, and yeasts. The percentage of reduction for the furniture and kitchen sponge samples was between 69.8 and 100 % as shown in (Table 4).

The microbicidal force of Ag NPs increases as the size decrease because of the large surface area subjected to the microbial contamination also the shape of the particles is also effective where Ag NPs may permeate into the microbial cells [50]. In our study, the small particle size (9.68 nm) of the biosynthesized Ag NPs elucidated their potent effect as an antimicrobial mediator [51]. One of the widespread mechanisms of the antibacterial action of Ag NPs is their capacity to bond with a thiol group of cysteine; that is, the building block of bacterial cell wall protein and this resulting in disruption of the enzymatic function of proteins and interruption of the cellular respiration chain. Also, Ag NPs may cause destroying of enzymes such as succinate dehydrogenase NADH [52].

Ag NPs may cause alterations in the regulation of genes expression and encode proteins of phosphorylation pathway that consist binding of a nucleophilic atom to phosphate excess in tyrosine OH group oxygen atom [53]. Ag NPs have a high antibacterial effect against various bacterial strains including the resistant bacteria [43]. The diversity in cell wall construction between Gram-positive and Gram-negative bacteria causes the difference in biocidal efficacy of Ag NPs against the two bacterial types [54]. Simultaneously, Ag NPs are powerful fungicides toward a broad spectrum of fungi including species such as *Candida*, *Saccharomyces*, and *Aspergillus* [7].

The alteration in the cell membrane structure might cause an increase in the permeability of the microbial cell, causing an uncontrolled transport process through the cytoplasmic membrane, and finally resulting in cell death. Furthermore, it has been suggested that the antimicrobial behavior of Ag NPs is due to the generation of the free radicals that induced membrane damage [55]. Further damage may possibly cause by interactions with DNA that consequently inhibit cell division and DNA replication causing cell death [56]. The possible mechanism that may describe the antibacterial effect of Ag NP treatment on the bacterial cells was illustrated in (Fig. 5).

**Table 4** Microbial total counts of furniture and kitchen sponge groups

| Furniture sponge groups | Bacterial total counts (CFU/mL) | | | | | | | | | | |
|---|---|---|---|---|---|---|---|---|---|---|---|
| | $10^{-1}$ | | $10^{-2}$ | | $10^{-3}$ | | $10^{-4}$ | | $10^{-5}$ | | Reduction rate (%) |
| | TC | Ag NPs TC | TC | Ag NPs TC | TC | Ag NPs TC | TC | Ag NPs TC | TC | Ag NPs TC | |
| G 1 | $81^{a} \pm 2.08$ | ND | $58^{a} \pm 2.08$ | ND | $49^{a} \pm 1.5$ | ND | $33^{b} \pm 2.08$ | ND | $17^{b} \pm 1.0$ | ND | 100 |
| G 2 | $92^{b} \pm 3.05$ | $8^{a} \pm 1.52$ | $73^{b} \pm 3.5$ | ND | $51^{b} \pm 1.52$ | ND | $40^{c} \pm 2.6$ | ND | $34^{d} \pm 1.0$ | ND | 97 |
| G 3 | $121^{e} \pm 2.08$ | ND | $80^{d} \pm 3.05$ | ND | $61^{c} \pm 1.52$ | ND | $49^{d} \pm 1.52$ | ND | $30^{c} \pm 4.04$ | ND | 100 |
| G 4 | $164^{f} \pm 2.6$ | ND | $120^{e} \pm 2.51$ | ND | $92^{d} \pm 3.05$ | ND | $63^{e} \pm 1.52$ | ND | $43^{f} \pm 3.51$ | ND | 100 |
| G 5 | $113^{d} \pm 2.51$ | ND | $85^{d} \pm 3.0$ | ND | $60^{c} \pm 3.21$ | ND | $49^{d} \pm 2.08$ | ND | $30^{c} \pm 0.57$ | ND | 100 |
| G 6 | $175^{g} \pm 3.6$ | $18^{b} \pm 1.0$ | $139^{f} \pm 3.7$ | $11 \pm 0.57$ | $101^{e} \pm 5.5$ | ND | $79^{f} \pm 1.15$ | ND | $55^{h} \pm 1.73$ | ND | 94.75 |
| G 7 | $99^{c} \pm 2.08$ | ND | $79^{c} \pm 1.0$ | ND | $61^{c} \pm 2.08$ | ND | $48^{d} \pm 2.51$ | ND | $39^{e} \pm 2.64$ | ND | 100 |
| G 8 | $177^{h} \pm 3.6$ | ND | $150^{g} \pm 2.8$ | ND | $112^{f} \pm 1.0$ | ND | $80^{g} \pm 2.3$ | ND | $51^{g} \pm 2.6$ | ND | 100 |
| G 9 | $210^{i} \pm 4.6$ | $34^{c} \pm 2.08$ | $170^{i} \pm 1.73$ | ND | $125^{g} \pm 3.0$ | ND | $99^{h} \pm 2.08$ | ND | $67^{i} \pm 2.3$ | ND | 94.91 |
| G 10 | $80^{a} \pm 3.05$ | ND | $72^{b} \pm 1.15$ | ND | $50^{b} \pm 1.0$ | ND | $28^{a} \pm 1.15$ | ND | $12^{a} \pm 0.57$ | ND | 100 |
| LSD | 6.4 | 9.3 | 5.00 | 0.10 | 4.92 | - | 3.50 | - | 3.62 | - | - |
| No fungal isolates were detected with furniture samples | | | | | | | | | | | |
| Kitchen sponge groups | Bacterial total counts (CFU/mL) | | | | | | | | | | |
| | $10^{-1}$ TC | Ag NPs TC | $10^{-2}$ TC | Ag NPs TC | $10^{-3}$ TC | Ag NPs TC | $10^{-4}$ TC | Ag NPs TC | $10^{-5}$ TC | Ag NPs TC | Reduction rate (%) |
| G 1 | $187^{b} \pm 2.5$ | $136^{b} \pm 1.52$ | $144^{b} \pm 1.90$ | $21^{b} \pm 1.0$ | $90^{b} \pm 1.73$ | ND | $68^{b} \pm 0.57$ | ND | $31^{b} \pm 0.57$ | ND | 69.86 |
| G 2 | $239^{c} \pm 2.6$ | $48^{c} \pm 1.52$ | $192^{c} \pm 2.5$ | $16^{a} \pm 0.57$ | $120^{c} \pm 2.5$ | ND | $88^{c} \pm 0.57$ | ND | $57^{c} \pm 1.52$ | ND | 90.81 |
| G 3 | $149^{a} \pm 1.0$ | $21^{a} \pm 1.52$ | $101^{a} \pm 2.5$ | ND | $79^{a} \pm 0.57$ | ND | $51^{a} \pm 1.0$ | ND | $28^{a} \pm 1.0$ | ND | 94.80 |
| | Fungal total counts (CFU/mL) | | | | | | | | | | |
| G 1 | M:$10^{c} \pm 0.57$ Y:ND | M: ND Y: ND | M: $6^{c} \pm 1.0$ Y:ND | M:ND Y:ND | M:$3^{b} \pm 0.28$ Y:ND | M: ND Y: ND | M: ND Y: ND | M: ND Y: ND | M: ND Y: ND | M: ND Y:ND | 100 |
| G 2 | M:$7^{a} \pm 0.57$ Y:$28^{d} \pm 1.52$ | M: ND Y: $5 \pm 0.28$ | M:$3^{a} \pm 0.56$ Y:$15^{d} \pm 0.57$ | M: ND Y: ND | M:ND Y:$4^{c} \pm 0.23$ | M: ND Y: ND | M: ND Y: ND | M:ND Y: ND | M: ND Y: ND | M:ND Y:ND | 100 89.34 |
| G 3 | M:$8^{b} \pm 1.15$ Y:$44^{e} \pm 1.15$ | M: ND Y: ND | M:$5^{b} \pm 0.57$ Y:$18^{e} \pm 0.51$ | M: ND Y: ND | M:$3^{b} \pm 0.57$ Y:$2^{a} \pm 0.57$ | M: ND Y: ND | M: ND Y: ND | M: ND Y: ND | M: ND Y: ND | M: ND Y: ND | 100 100 |
| **LSD** | 4.34 | - | 2.67 | - | 1.00 | - | - | - | - | - | - |

TC: microbial total counts of untreated sponge samples (control); Ag NPs TC: microbial total counts of Ag NP-treated sponge samples; M: molds; Y: yeast; ND: not detected. The results are represented as mean ± SD; LSD: least significant difference. Means bearing different superscripts differ significantly ($p < 0.05$) by Duncan's multiple range test

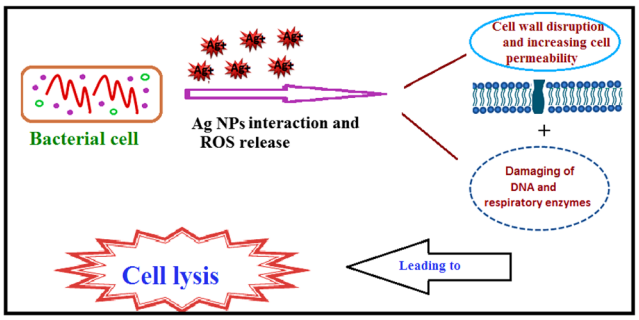


**Fig. 5** The possible mechanism of Ag NP treatment on the bacterial cells causing the alteration in the cell membrane structure, interactions with DNA that consequently inhibit cell division and finally resulting in cell death

### Enumeration of the Household Sponge Isolates

The enumeration of various bacterial species on their specific media showed that Ag NP treatment has different effects against diverse bacterial species. The inhibition percentage of *Salmonella* spp., the causal microorganism of the most food poising cases, was 100%. On the other hand, *Staphylococcus* spp. growth was reduced by 73.49 %, and the Gram-negative bacteria count was reduced by 65.12 %, while coliform bacteria were the less reduction percentage (54.3 %) as illustrated in Table 5. As consequence, the rest of the antibacterial tests were performed against *Salmonella* spp. and *Staphylococcus* spp. because they have the highest reduction rate.

Our results have been proved by previous studies where Ag NPs synthesized by microorganisms were an efficient antimicrobial factor toward *Klebsiella pneumoniae*, *Escherichia coli*, *Salmonella infantis*, *Proteus mirabilis*, and *Bacillus subtilis*. These bacterial strains were not capable to resistant the biocolloidal silver treatment [57]. Comparative research was investigated by [58] who indicated strong antimicrobial activity of Ag NPs synthesized by the bacterial strain *Pseudomonas aeruginosa* ATCC with particle size 33–300 nm against *Salmonella typhimurium*, *Escherichia coli*, *Staphylococcus aureus*, *Acinetobacter baumannii*, and *Candida albicans*.

Also, [59] revealed that Ag NPs induced cell wall thinning and increased permeability of Gram-positive bacteria cells which reduced stabilization of peptidoglycan layer causing lysis of the bacterial cell. Moreover, Gram-positive bacteria cell wall contains teichoic acids that may bind to Ag NPs to weak the bacterial cell wall [60].

Finally, the biosynthesis of Ag NPs with *G. deliquescens* and 25.0 kGy gamma irradiation was an eco-friendly approach. It can be noticed that the biosynthesized Ag NPs has an effective function in reducing or completely inhibiting the microbial contamination in the tested household sponge samples. Therefore, Ag NPs may be applied as a potent disinfectant of household sponge.

## The Antibacterial Potency of Ag NPs on *Salmonella* spp. and *Staphylococcus* spp.

### Disk Diffusion Test

The disk diffusion test was carried out to assess the antibacterial action of Ag NPs (50.0 μg/mL), positive control (Amoxicillin/clavulanate 20/10 μg/mL), and negative control (fungal cell-free supernatant) against *Salmonella* spp. and *Staphylococcus* spp. as shown in Fig.6a. The results illustrated that the antibacterial activity was represented by Ag NPs and the antibiotic disks but no antibacterial activity was recognized for the fungal cell-free supernatant. Ag NPs have the greatest zone of inhibition upon *Salmonella* spp. (14 ± 0.25 mm) compared with the *Staphylococcus* spp. (12.3 ± 0.34 mm) while the

**Table 5** Enumeration of different microbial species of household sponge samples

| Microbes | The count percentage | | Reduction rate (%) |
|---|---|---|---|
| | TC | Ag NPs count | |
| Coliform bacteria | $13.34^{b} \pm 0.320$ | $6.09^{b} \pm 0.047$ | 54.34 |
| *Staphylococcus* spp. | $21.5^{f} \pm 3.60$ | $5.7^{f} \pm 1.52$ | 73.49 |
| *Salmonella* spp. | $1.26^{a} \pm 0.036$ | $0.00^{a} \pm 0.00$ | 100 |
| Gram-negative | $25^{c} \pm 0.577$ | $8.72^{c} \pm 0.312$ | 65.12 |
| LSD | 11.45 | 2.60 | |

The results are described as mean ± SD. LSD: least significant difference. Means bearing different superscripts differ significantly ($p < 0.05$) by Duncan's multiple range test

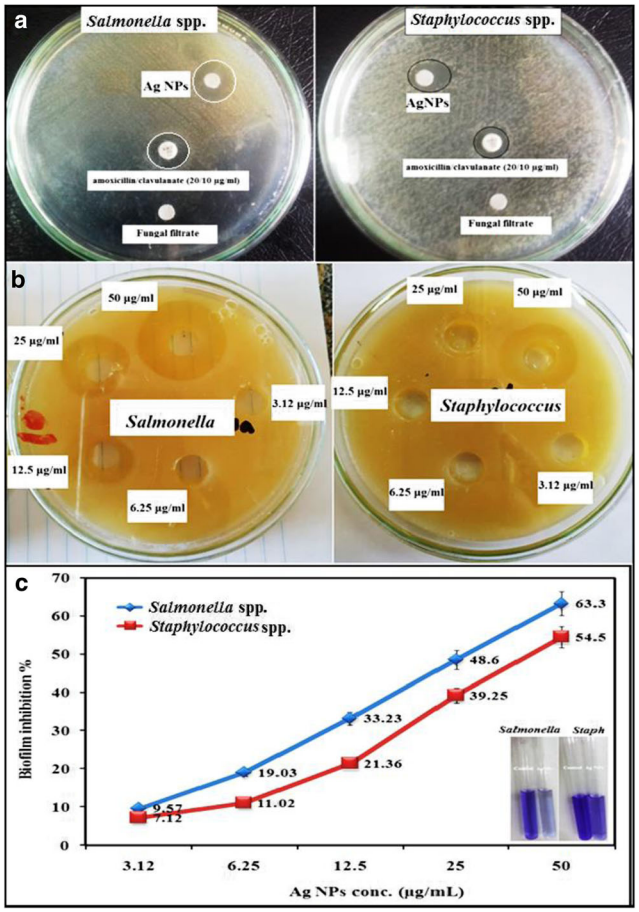


**Fig. 6** The antibacterial of the biogenic Ag NPs (50.0 µg/mL) against the isolated bacteria *Salmonella* spp.,and *Staphylococcus* spp. by **a** disk diffusion method performed zone of inhibition, **b** MIC and MBC analysis, and **c** The antibiofilm activity test (A biofilm is an assemblage of microbial cells that is irreversibly associated with a surface and enclosed in a matrix of primarily polysaccharide material)

antibiotic, amoxicillin/clavulanate 20/10 (µg/mL) has an inhibition zone (11.67 ± 0.24 mm) for *Salmonella* spp. and (9.67 ± 0.125 mm) for *Staphylococcus* spp.

## Analysis of MIC and MBC

By implementing minimum inhibitory concentration analysis, MIC of Ag NPs that synthesized using 25.0 kGy gamma irradiated *G. deliquescens* cell-free supernatant was determined on the *Salmonella* spp. and *Staphylococcus* spp. This experiment was conducted on Ag NPs at concentrations 50, 25, 12.5, 6.25, and 3.12 µg/mL by well diffusion method and the results have been reported in Fig.6b. The MIC assessment of Ag NPs toward *Salmonella* spp. was 6.25 ± 0.354 µg/mL and MBC was 12.5 ± 0.404 µg/mL, while MIC and MBC values of Ag NPs against *Staphylococcus* spp. were 12.5 ± 0.305 and 25 ± 0.346 µg/mL, respectively. Ag NPs have dual behavior acting as bacteriostatic in their lower concentration, on the other hand, behaving as bactericidal at the higher concentration. The antibacterial force of Ag NPs against Gram-negative bacteria, *Salmonella* spp. was more powerful than against Gram-positive bacteria, *Staphylococcus* spp. The whole inhibition of bacteria is preceded by raising the concentration of Ag NPs (Fig. 6b).

## Biofilm Formation and Antibiofilm Activity of Ag NPs

Ag NPs were used in different concentrations 3.12, 6.25, 12.5, 25.0, and 50.0 µg/mL to assess their potency to inhibit the biofilm formation of *Salmonella* spp. and *Staphylococcus* spp. It was clearly shown in Fig.6c that, by increasing the concentration of Ag NPs the biofilm inhibition rate increased. The antibiofilm activity of Ag NPs was highest at the concentration of 50 µg/mL registering 63.3 % for *Salmonella* spp. and 54.5 % for *Staphylococcus* spp. Since the antimicrobial potency of NPs is greatly depending on the particles size, the smaller dimensions of Ag NPs (9.68 nm) gives powerful antibiofilm activity upon *Salmonella* spp. and *Staphylococcus* spp.

A biofilm is an assemblage of microbial cells that is irreversibly associated (not removed by gentle rinsing) with a surface and enclosed in a matrix of primarily polysaccharide material [61]. The raised affinity of Ag NPs to sufur and phosphorus is the major basis of its antibacterial characteristics where sulfur and phosphorus were detected in abundance in

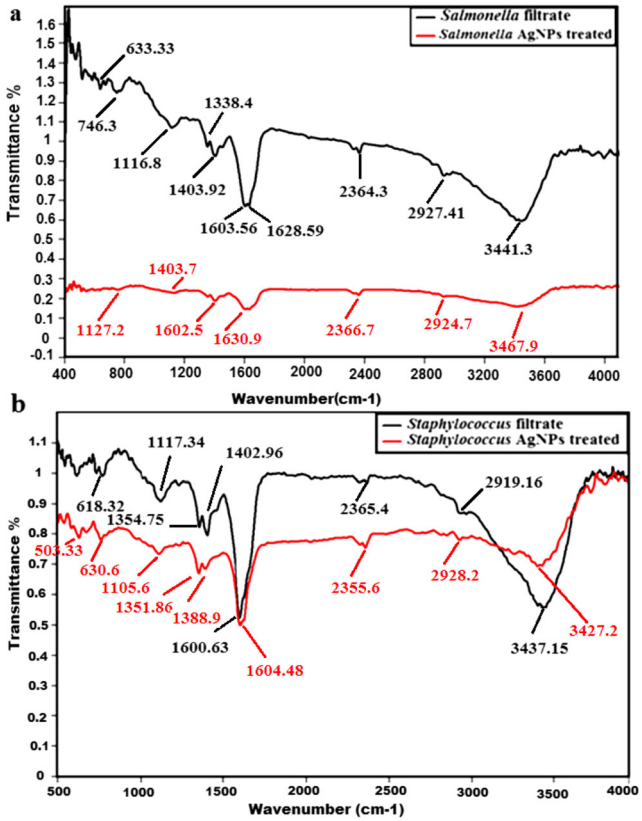


**Fig. 7** Comparative FTIR spectrum of untreated and Ag NP-treated filtrates of **a** *Salmonella* spp. and **b** *Staphylococcus* spp. showed the reduction of the transmittance percentage with Ag NP treatment for all vibration bands demonstrating the decrease in vital components of the bacterial cells as protein content, phospholipids, and polysaccharides

the bacterial cell membrane. Several studies have reported that *Salmonella* spp. and *Staphylococcus* spp. have a physical powerful capacity to form bacterial adhesion and were grouped as strong biofilm formers [62].

It has been documented that biofilms are a frequent common infections source and almost 80% of unrelenting bacterial infections in the world were actually associated with biofilms [63].

There are several mechanisms that explained how the biofilm is synthesized on the surface, like the presence of genes accountable for the adhesion route and the production of the extracellular polymeric substance. The environmental conditions may also affect biofilm formation [64].

The environmental conditions and expression of specific genes induced by adhesion may theoretically control the metabolic activity of biofilms [65]. The low cellular metabolism gives resistance to the antimicrobial agents that proceed during bacterial growth.

## Comparison of the Fourier-Transform Infrared Spectra

The FTIR analysis was performed in order to exhibit the spectral changes between the untreated (used as control) and Ag NP-treated bacterial filtrates of *Salmonella* spp. and *Staphylococcus* spp. FTIR spectral data of *Salmonella* spp. and *Staphylococcus* spp. were implemented over the frequency range of 400–4000 $cm^{-1}$. As could be obvious from Fig. 7 a&b, the untreated (control) and Ag NPtreatment spectra noticeably varied in the peaks height, the bandwidths, the intensity percentage, and the values of FTIR bands frequency. The treatment with Ag NPs mainly reduced the transmittance percentage for all vibration bands demonstrating the decrease in vital components of the bacterial cells as protein content, phospholipids, and polysaccharides.

The FTIR stretching vibration intensity was higher in the untreated bacterial filtrates than the Ag NP-treated filtrates for both *Salmonella* spp. and *Staphylococcus* spp. Spectral variations were so significant across the whole spectral range, where there were some observable disparity between spectra particularly at (1200 to 1500 $cm^{-1}$) the region of phospholipids DNA-RNA, (1500 to 1700 $cm^{-1}$) the region of proteins and amides I and II), (900 to 1200 $cm^{-1}$) the region of polysaccharides, and at (600 to 900 $cm^{-1}$) the region of fingerprint [66]. Also, a vibration band at 1628 $cm^{-1}$that represented amide I of the protein alpha-helical structure was extremely reduced. The vigorous and wide-range absorption band at 3300 $cm^{-1}$ should be assigned to N-H stretching vibrations of the components of nucleic acids as guanine, adenine, and/or cytosine, and may to OH groups that probably adsorbed on the molecules of nucleic acids [67]. In addition**,** in each acyl chain, minimize the value of the CH stretching band intensity at 2928 $cm^{-1}$ in the spectrum of the Ag NPs treated bacteria indicating lowering in the methyl groups number compared to untreated bacteria [68]. Previous researchers have demonstrated that the concentration of Ag NPs may affect their antimicrobial action and was intimately relevant to the generation of pits that appear in the microbial cell wall [69]. Additional, Ag NPs with negative charge may accumulate in the bacterial membrane causing an increase in the permeability of the membrane.

## Appreciation of the action of Ag NPs on the bacteria by the scanning electron microscope

The electron micrographs by SEM of *Salmonella* spp. and *Staphylococcus* spp. cells treated and untreated with Ag NPs were represented in Fig. 8. The micrograph through SEM (Fig. 8a) attested the surface of untreated *Salmonella* spp. cells was smooth and appeared as usual rod shape, while cells treated with 50.0 μg/mL of Ag NPs (Fig 6b) were hardly damaged and showed serious morphological changes. Some cells exhibited large infiltration, while other cells showed severe distortion and fragmentation. SEM images of *Staphylococcus* spp. cells indicated that cells were injured as a result of the adherence of bacterial cells to Ag NPs (Fig.8 c&d). There were many fragments on the cell surface considering the antimicrobial activity of Ag NPs on the permeability

of the *Staphylococcus* spp. cell membrane. This may be due to when metal nanoparticles come into contact with microbial cells, they interact with the outer surface of the plasma membrane causing disruption of its structure and change its permeability [70].

From SEM observation; the morphological destruction of the *Staphylococcus* spp. (Gram-positive bacteria) was weaker than *Salmonella* spp. (Gram-positive bacteria). The Gram-negative bacteria cell envelope formed of an outer membrane, followed by few nanometers peptidoglycan layer, and finally cell membrane while the Gram-positive cell envelope formed of lipoteichoic acid including thick peptidoglycan many layers with a high thickness (30–100 nm), and lastly cell membrane. This diversity was possibly attributable to the variation of the peptidoglycan layer of Gram-positive and Gram-negative bacteria where the defense against antibacterial factors like antibiotics, and chemicals is the fundamental role of the peptidoglycan layer. In addition, the great diameter of the peptidoglycan layer of Gram-positive bacteria may play an efficient impact against pits or ROS formation as a result of Ag NP treatment [71].

Ag NPs nanoparticles are known for their stability as an antimicrobial. Ag NPs have a longer-lasting effect and higher efficiency than ordinary antiseptics due to the properties of nanomaterials as they have the large surface area and a very small partial size so that it is easy to enter between sponge particles and continues to exist for longer periods. Ag NPs act as an insulator and protection from microbial contamination as well as being used as an antiseptic after the occurrence of contamination and thus outperforms its companion of bulk chemicals that used as disinfectants cleaner. But after a period of time the contamination may occur again because of the continuous renewal of the causes of contamination. The contaminants are ubiquitous and may likely result from normal food preparation. Overall, the source of many of these organisms is likely to be the food itself including lamb, beef and seafood. A high potential for the transfer of microbial contaminants from the sponge to other kitchen surfaces or during daily uses of furniture sponge may happen with a great opportunity. So, if this happens we will re-renew the treatment again taking into consideration that the silver metal taken in the treatment is minimal concentrations under the safety limit allowed according to numerous researches so it is considered to be negligible.

## Conclusion

In conclusion, we can suppose that accepting silver nanoparticles may restrict environmental pollution and extravagant usage of chemical compounds in household sponge decontamination. Synthesis of Ag NPs by *Gliocladium deliquescens* cell-free supernatant and gamma irradiation was considered a promising technique. Ag NPs seriously reduced the microbial contamination and improved proprieties of the household

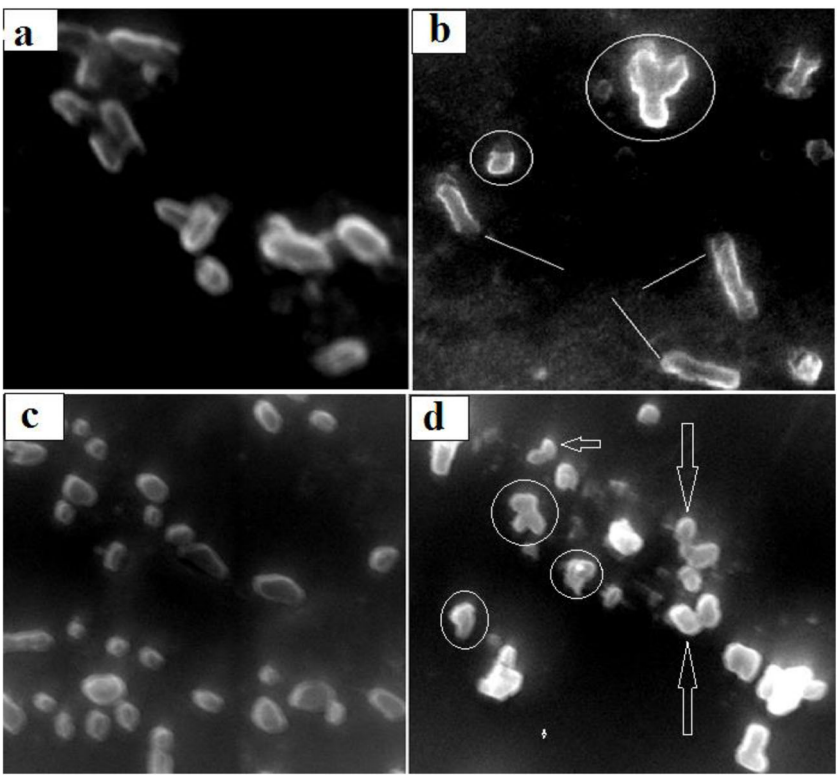


**Fig. 8** Scanning electron microscope images of **a** the untreated *Salmonella* spp. cells (control), **b** *Salmonella* spp. cells treated with Ag NPs (50.0 μg/mL), **c** the untreated *Staphylococcus* spp. cells (control), and **d** *Staphylococcus* spp. cells treated with Ag NPs (50.0 μg/mL). Circles and arrows refer to large infiltration, malformation and sever distortion and fragmentation of the Ag NPs treated bacteria cells

sponge. It is predictable that Ag NP application at low concentrations will be frugal, eco-friendly, and reduce administration costs.

**Acknowledgments** The authors would like to thank P.I. Prof. Dr. Ahmed Ibrahim El-Batal, Drug Microbiology Lab, Drug Radiation Research Department, NCRRT, Cairo, Egypt, for supporting this study. Also, the authors thank greatly Dr. Gharieb Saied El-Sayyad for his valuable guidance during this investigation.

**Compliance with Ethical Standards** Permissions were obtained for collection of samples from the responsible authorities of the household were indicated previously.

**Conflict of Interest** The authors declare that they have no conflict of interest.

**Research involving Human Participation and/or Animals** Not applicable.

**Informed consent** Applicable.

**Ethical approval** Applicable.

## References

1. Guo J-Z, Cui H, Zhou W, Wang W (2008) Ag nanoparticle-catalyzed chemiluminescent reaction between luminol and hydrogen peroxide. J Photochem Photobiol 193(2-3):89–96
2. Lansdown AB (2006) Silver in health care: antimicrobial effects and safety in use. In: Biofunctional textiles and the skin, vol 33. Karger Publishers, pp 17–34
3. Mueller NC, Nowack B (2008) Exposure modeling of engineered nanoparticles in the environment. Environ Sci Technol 42(12): 4447–4453
4. El-Batal AI, El-Sayyad GS, Mosallam FM, Fathy RM (2019) *Penicillium chrysogenum*-mediated mycogenic synthesis of copper oxide nanoparticles using gamma rays for in vitro antimicrobial activity against some plant pathogens. J Clust Sci:1–12
5. Sondi I, Salopek-Sondi B (2004) Silver nanoparticles as antimicrobial agent: a case study on E. coli as a model for Gram-negative bacteria. J Colloid Interface Sci 275(1):177–182
6. Jung WK, Koo HC, Kim KW, Shin S, Kim SH, Park YH (2008) Antibacterial activity and mechanism of action of the silver ion in *Staphylococcus aureus* and *Escherichia coli*. Appl Environ Microbiol 74(7):2171–2178
7. Wright J, Lam K, Hansen D, Burrell R (1999) Efficacy of topical silver against fungal burn wound pathogens. Am J Infect Control 27(4):344–350
8. Okafor F, Janen A, Kukhtareva T, Edwards V, Curley M (2013) Green synthesis of silver nanoparticles, their characterization, application and antibacterial activity. Int J Environ Res Public Health 10(10):5221–5238
9. Bonsak J, Mayandi J, Thøgersen A, Stensrud Marstein E, Mahalingam U (2011) Chemical synthesis of silver nanoparticles for solar cell applications. Phys Status Solidi 8(3):924–927
10. Zhang G, Liu Y, Gao X, Chen Y (2014) Synthesis of silver nanoparticles and antibacterial property of silk fabrics treated by silver nanoparticles. Nanoscale Res Lett 9(1):216
11. Ismail A-WA, Sidkey NM, Arafa RA, Fathy RM, El-Batal AI (2016) Evaluation of in vitro antifungal activity of silver and selenium nanoparticles against *Alternaria solani* caused early blight disease on potato. Br Biotechnol J 12(3):1
12. Cho I-H, Ku S (2017) Current technical approaches for the early detection of foodborne pathogens: Challenges and opportunities. Int J Mol Sci 18(10):2078
13. Cinti S, Volpe G, Piermarini S, Delibato E, Palleschi G (2017) Electrochemical biosensors for rapid detection of foodborne Salmonella: A critical overview. Sensors 17(8):1910
14. El-Batal A, El-Baz A, Abo Mosalam F, Tayel A (2013) Gamma irradiation induces silver nanoparticles synthesis by *Monascus purpureus*. J Chem Pharm Res 5(8):1–15
15. El-Batal AI, El-Sayyad GS, El-Ghamery A, Gobara M (2017) Response surface methodology optimization of melanin production by Streptomyces cyaneus and synthesis of copper oxide nanoparticles using gamma radiation. J Clust Sci 28(3):1083–1112
16. Liao S, Zhang Y, Pan X, Zhu F, Jiang C, Liu Q, Cheng Z, Dai G, Wu G, Wang L (2019) Antibacterial activity and mechanism of silver nanoparticles against multidrug-resistant *Pseudomonas aeruginosa*. Int J Nanomedicine 14:1469
17. El-Batal AI, Sidkey NM, Ismail A, Arafa RA, Fathy RM (2016) Impact of silver and selenium nanoparticles synthesized by gamma irradiation and their physiological response on early blight disease of potato. J Chem Pharm Res 8(4):934–951
18. Golińska P, Wypij M, Rathod D, Tikar S, Dahm H, Rai M (2016) Synthesis of silver nanoparticles from two acidophilic strains of Pilimelia columellifera subsp. pallida and their antibacterial activities. J Basic Microbiol 56(5):541–556
19. Josephson K, Rubino J, Pepper I (1997) Characterization and quantification of bacterial pathogens and indicator organisms inhousehold kitchens with and without the use of a disinfectant cleaner. J Appl Microbiol 83(6):737–750
20. Szita G, Gyetvai B, Szita J, Gyenes M, Solymos N, Soos L, Hajos A, Toth P, Bernáth S (2008) Synthetic culture media evaluated for the detection of coliform bacteria in milk, cheese and egg melange. Acta Vet Brno 77(1):143–147
21. Stiles M (1977) Reliability of selective media for recovery of staphylococci from cheese. Journal of Food Protection 40(1):11–16
22. Nesa M, Khan M, Alam M (2011) Isolation, identification and characterization of *Salmonella serovars* from diarrhoeic stool samples of human. Bangl J Vet Med 9(1):85–93
23. Horvath R, Ropp M (1974) Mechanism of action of eosin-methylene blue agar in the differentiation of *Escherichia coli* and *Enterobacter aerogenes*. Int J Syst Evol Microbiol 24(2):221–224
24. Lkhagvajav N, Koizhaiganova M, Yasa I, Çelik E, Sari Ö (2015) Characterization and antimicrobial performance of nano silver coatings on leather materials. Braz J Microbiol 46(1):41–48
25. El-Sayyad GS, Mosallam FM, El-Batal AI (2018) One-pot green synthesis of magnesium oxide nanoparticles using *Penicillium chrysogenum* melanin pigment and gamma rays with antimicrobial activity against multidrug-resistant microbes. Adv Powder Technol 29(11):2616–2625
26. Maiti S, Krishnan D, Barman G, Ghosh SK, Laha JK (2014) Antimicrobial activities of silver nanoparticles synthesized from *Lycopersicon esculentum* extract. Anal Sci Tech 5(1):40
27. Maksoud MA, El-Sayyad GS, Ashour A, El-Batal AI, Elsayed MA, Gobara M, El-Khawaga AM, Abdel-Khalek E, El-Okr M (2019) Antibacterial, antibiofilm, and photocatalytic activities of metals-substituted spinel cobalt ferrite nanoparticles. Microb Pathog 127: 144–158
28. El-Nemr KF, Mohamed HR, Ali MA, Fathy RM, Dhmees AS (2019) Polyvinyl alcohol/gelatin irradiated blends filled by lignin as green filler for antimicrobial packaging materials. Int J Environ An Ch 1–25
29. Puzey K, Gardner P, Petrova V, Donnelly C, Petrucci G (2008) Automated species and strain identification of bacteria in complex matrices using FTIR spectroscopy. In: Chemical, biological,

radiological, nuclear, and explosives (CBRNE) sensing IX, vol 3. International Society for Optics and Photonics, pp 1–9
30. Murtey MD, Ramasamy P (2016) Sample preparations for scanning electron microscopy–life sciences. Modern electron microscopy in physical and life sciences. M. Janecek. InTech, In
31. Kim H-Y (2014) Analysis of variance (ANOVA) comparing means of more than two groups. Restorative Dentistry & Endodontics 39(1):74–77
32. El-Batal AI, Mosallam FM, El-Sayyad GS (2018) Synthesis of metallic silver nanoparticles by fluconazole drug and gamma rays to inhibit the growth of multidrug-resistant microbes. J Clust Sci 29(6):1003–1015
33. Korbekandi H, Iravani S, Abbasi S (2012) Optimization of biological synthesis of silver nanoparticles using *Lactobacillus casei* subsp. casei. J Chem Technol Biotechnol 87(7):932–937
34. Baraka A, Dickson S, Gobara M, El-Sayyad GS, Zorainy M, Awaad MI, Hatem H, Kotb MM, Tawfic A (2017) Synthesis of silver nanoparticles using natural pigments extracted from Alfalfa leaves and its use for antimicrobial activity. Chem Pap 71(11): 2271–2281
35. Mohanpuria P, Rana NK, Yadav SK (2008) Biosynthesis of nanoparticles: technological concepts and future applications. J Nanoparticle Res 10(3):507–517
36. Abd-Elnaby HM, Abo-Elala GM, Abdel-Raouf UM, Hamed MM (2016) Antibacterial and anticancer activity of extracellular synthesized silver nanoparticles from marine *Streptomyces rochei* MHM13. Egypt J Aquat Res 42(3):301–312
37. Mosallam FM, El-Sayyad GS, Fathy RM, El-Batal AI (2018) Biomolecules-mediated synthesis of selenium nanoparticles using *Aspergillus oryzae* fermented Lupin extract and gamma radiation for hindering the growth of some multidrug-resistant bacteria and pathogenic fungi. Microb pathog 4(11):1341–1363
38. Tulve NS, Stefaniak AB, Vance ME, Rogers K, Mwilu S, LeBouf RF, Schwegler-Berry D, Willis R, Thomas TA, Marr LC (2015) Characterization of silver nanoparticles in selected consumer products and its relevance for predicting children's potential exposures. Int J Hyg Environ Health 218(3):345–357
39. Mohammadian A, Shojaosadati S, Habibi Rezaee M (2007) Fusarium oxysporum mediates photogeneration of silver nanoparticles. Sci Iran 14(4):323–326
40. Chowdhury S, Yusof F, Faruck MO, Sulaiman N (2016) Process optimization of silver nanoparticle synthesis using response surface methodology. Procedia Eng 148:992–999
41. Le Caër S (2011) Water radiolysis: influence of oxide surfaces on H2 production under ionizing radiation. Water 3(1):235–253
42. Madhukumar R, Byrappa K, Wang Y, Sangappa Y (2018) Effect of gamma irradiation on synthesis and characterization of bionanocomposite SF/Ag nanoparticles. Radiat Eff Defect S :1–7
43. El-Batal A, Haroun BM, Farrag AA, Baraka A, El-Sayyad GS (2014) Synthesis of silver nanoparticles and incorporation with certain antibiotic using gamma irradiation. Br J Pharm Res 4(11): 1341–1363
44. Ammar H, El-Desouky T (2016) Green synthesis of nanosilver particles by Aspergillus terreus HA1N and *Penicillium expansum* HA2N and its antifungal activity against mycotoxigenic fungi. J Appl Microbiol 121(1):89–100
45. El-Baz AF, El-Batal AI, Abomosalam FM, Tayel AA, Shetaia YM, Yang ST (2016) Extracellular biosynthesis of anti-Candida silver nanoparticles using *Monascus purpureus*. J Basic Microbiol 56(5): 531–540
46. Priyadarshini S, Gopinath V, Priyadharsshini NM, MubarakAli D, Velusamy P (2013) Synthesis of anisotropic silver nanoparticles using novel strain, *Bacillus flexus* and its biomedical application. Colloid Surface B 102:232–237
47. Kumar V, Yadav SC, Yadav SK (2010) *Syzygium cumini* leaf and seed extract mediated biosynthesis of silver nanoparticles and their characterization. J Chem Technol Biotechnol 85(10):1301–1309
48. Suresh AK, Pelletier DA, Wang W, Broich ML, Moon J-W, Gu B, Allison DP, Joy DC, Phelps TJ, Doktycz MJ (2011) Biofabrication of discrete spherical gold nanoparticles using the metal-reducing bacterium *Shewanella oneidensis*. Acta Biomater 7(5):2148–2152
49. Gudikandula K, Vadapally P, Charya MS (2017) Biogenic synthesis of silver nanoparticles from white rot fungi:Their characterization and antibacterial studies. OpenNano 2:64-78
50. Adebayo-Tayo BC, Popoola AO, Ajunwa OM (2017) Bacterial synthesis of silver nanoparticles by culture free supernatant of lactic acid bacteria isolated from fermented food samples. Biotechnol J Int 19(1):1–13
51. Oza G, Pandey S, Shah R, Sharon M (2012) Extracellular fabrication of silver nanoparticles using *Pseudomonas aeruginosa* and its antimicrobial assay. Pelagia Res Lib Adv Appl Sci Res 3(3):1778–1783
52. Pulit-Prociak J, Banach M (2016) Silver nanoparticles–a material of the future …? Open Chem 14(1):76–91
53. Park H-J, Kim JY, Kim J, Lee J-H, Hahn J-S, Gu MB, Yoon J (2009) Silver-ion-mediated reactive oxygen species generation affecting bactericidal activity. Water Res 43(4):1027–1032
54. Alaqad K, Saleh T (2016) Gold and silver nanoparticles: synthesis methods, characterization routes and applications towards drugs. J Environ Anal Toxicol 6(384):2161–0525.1000384
55. Dakal TC, Kumar A, Majumdar RS, Yadav V (2016) Mechanistic basis of antimicrobial actions of silver nanoparticles. Front Microbiol 7:1831
56. Morones JR, Frey W (2007) Environmentally sensitive silver nanoparticles of controlled size synthesized with PNIPAM as a nucleating and capping agent. Langmuir 23(15):8180–8186
57. Buszewski B, Railean-Plugaru V, Pomastowski P, Rafinska K, Szultka-Mlynska M, Kowalkowski T (2017) Antimicrobial effectiveness of bioactive silver nanoparticles synthesized by *Actinomycetes* HGG16n Strain. Curr Pharm Biotechnol 18(2): 168–176
58. Peiris MK, Gunasekara CP, Jayaweera PM, Arachchi ND, Fernando N (2017) Biosynthesized silver nanoparticles: are they effective antimicrobials? Memórias do Instituto Oswaldo Cruz 112(8):537–543
59. Romero-Urbina DG, Lara HH, Velázquez-Salazar JJ, Arellano-Jiménez MJ, Larios E, Srinivasan A, Lopez-Ribot JL, Yacamán MJ (2015) Ultrastructural changes in methicillin-resistant *Staphylococcus aureus* induced by positively charged silver nanoparticles. Beilstein J Nanotechnol 6:2396
60. Kawai S, Phan TA, Kono E, Harada K, Okai C, Fukusaki E, Murata K (2009) Transcriptional and metabolic response in yeast *Saccharomyces cerevisiae* cells during polyethylene glycol-dependent transformation. J Basic Microbiol 49(1):73–81
61. Donlan RM (2002) Biofilms: microbial life on surfaces. Emerg infect dis 8(9):881–890
62. Iñiguez-Moreno M, Gutiérrez-Lomelí M, Guerrero-Medina PJ, Avila-Novoa MG (2018) Biofilm formation by *Staphylococcus aureus* and *Salmonella* spp. under mono and dual-species conditions and their sensitivity to cetrimonium bromide, peracetic acid and sodium hypochlorite. Braz J Microbiol 49(2):310–319
63. Janssens JC, Steenackers H, Robijns S, Gellens E, Levin J, Zhao H, Hermans K, De Coster D, Verhoeven TL, Marchal K (2008) Brominated furanones inhibit biofilm formation by *Salmonella enterica* serovar Typhimurium. Appl Environ Microbiol 74(21): 6639–6648
64. Duarte A, Alves AC, Ferreira S, Silva F, Domingues FC (2015) Resveratrol inclusion complexes: antibacterial and anti-biofilm activity against *Campylobacter* spp. and Arcobacter butzleri. Food Res Int 77:244–250

65. O'toole GA, Kolter R (1998) Flagellar and twitching motility are necessary for *Pseudomonas aeruginosa* biofilm development. Mol Microbiol 30(2):295–304
66. Preisner O, Guiomar R, Machado J, Menezes JC, Lopes JA (2010) Application of Fourier transform infrared spectroscopy and chemometrics for differentiation of *Salmonella enterica* serovar *Enteritidis* phage types. Appl Environ Microbiol 76(11):3538–3544
67. Filip Z, Hermann S, Demnerová K (2009) FT-IR spectroscopic characteristics of differently cultivated *Escherichia coli*. Czech J Food Sci 26(6):458–463
68. Kamnev A, Antonyuk L, Tugarova A, Tarantilis P, Polissiou M, Gardiner P (2002) Fourier transform infrared spectroscopic characterisation of heavy metal-induced metabolic changes in the plant-associated soil bacterium *Azospirillum brasilense* Sp7. J Mol Struct 610(1-3):127–131
69. Mishra P, Tyagi S, Tripathi D (2019) Comparative evaluation of silver nanoparticles and 5.25% sodium hypochlorite for rapid chairside decontamination of artificially infected gutta-percha with *Escherichia coli*: an in vitro Study. Density Med Res 7:1–23
70. Abdel-Rahman HA, Awad EH, Fathy RM (2019) Effect of modified nano zinc oxide on physico-chemical and antimicrobial properties of gamma-irradiated sawdust/epoxy composites. J Compos Mater. https://doi.org/10.1177/0021998319863835
71. Kim, S. H., Lee, H. S., Ryu, D. S., Choi, S. J., and Lee, D. S. (2011) Antibacterial Activity of Silver-nanoparticles Against Staphylococcus aureus and Escherichia coliKorean J. Microbiol. Biotechnol. 39, 77–85.